CHEMISTRY OF MATERIALS

Perspective

pubs.acs.org/cm

Postsynthetic Doping Control of Nanocrystal Thin Films: Balancing Space Charge to Improve Photovoltaic Efficiency

Jesse H. Engel and A. Paul Alivisatos*

Material Sciences Division, Lawrence Berkeley National Laboratory, Berkeley, California 94720, United States

Department of Materials Science, University of California, Berkeley, California 94720, United States

ABSTRACT: A semiconductor nanocrystal film is a unique class of nanocomposite, whose collective properties are determined by those of its constituents. Colloidal synthetic methods offer precise size control and finely tuned optical properties via quantum confinement, while recent improvements in charge transport through films have led to a variety of optoelectronic applications. However, understanding the role of defects and impurities in doping, crucial for optimizing device performance, has remained more elusive. In this perspective, we review recent progress in understanding and controlling the doping of semiconductor nanocrystal thin films, with a special focus on its relevance to photovoltaic applications. We highlight an array of postsynthetic techniques based on stoichiometric control, metal impurity incorporation, and electrochemical charging. We conclude with a review of the state of the art for nanocrystal photovoltaics, and propose the use of controlled doping and charge balance as a pathway to higher device efficiencies.

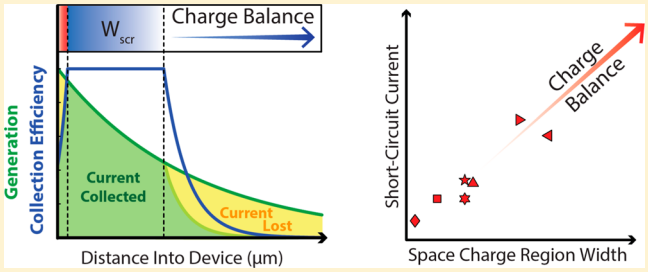

KEYWORDS: *quantum dots, nanocrystals, doping, photovoltaics, compensation*

INTRODUCTION

Colloidal nanocrystal photovoltaics are a young, but quickly developing technology. While the world record power conversion efficiency currently sits at a modest 7%,[1] it is increasing at a rate that is among the highest of all photovoltaic (PV) technologies (+1%/year).[2] Many of the innovations underpinning these improvements exploit the ability to tune the effective properties of nanocrystal thin films through chemical modification of their nanoscale constituents. Optimized photovoltaics require precise control over the optical properties, transport properties, and chemical potential of the semiconductor active layer,[3] and despite the disorder and heterogeneity present within nanocrystal films, the effective medium properties can be approximated as uniform when the length scale of interest is much larger than that of the nanoscale variations.[4]

The optical properties of a nanocrystal film, including permittivity, absorption coefficient and bandgap, are dramatically altered with nanocrystal size and capping ligand.[5−8] Quantitative understanding of the size dependent optical properties of individual nanocrystals has emerged from the ability to synthesize samples of high monodispersity in solution.[9] Through solution deposition techniques, this fine level of synthetic control can be leveraged to fabricate thin films with similar control over their optical properties. For example, films composed of nanocrystals of a single material, lead selenide (PbSe), can exhibit bandgaps from a bulk-like 0.3 eV to a highly confined 2.2 eV, as the crystal diameter is reduced down to 1 nm.[6] Since the wavelength of light is much larger than variations in the film, the far-field optical properties of the nanocomposite are given by effective medium theory.[10,11]

For optoelectronic applications, thin films must also efficiently transport charge. A film of colloidally synthesized nanocrystals is inherently a granular material comprised of void space, capping ligands, and the nanocrystals themselves. Conduction is inhibited by the long insulating organic ligands used for colloidal stability during synthesis, frequently trioctylphosphine or oleate.[12,13] Layer-by-layer ligand exchange techniques can be used to replace these native ligands with shorter ones, such as ethanedithiol (EDT),[14] thiocyanate (SCN),[15] hydrazine (N_2H_4),[16] mercaptopropionic acid (MPA),[17] and even atomic capping species such as chalcogenides[18] or halides.[19] These exchanges reduce interparticle spacing and promote transport, increasing mobilities by several of magnitude at the expense of induced structural disorder throughout the nanocrystal superlattice because of volume contraction.[14] However, these glassy superlattices still exhibit uniform transport characteristics, such as conductivity and mobility, if they are sufficiently above the percolation threshold such that inhomogeneities in interparticle transfer rates are negated by dominant percolation paths.[20]

Special Issue: Celebrating Twenty-Five Years of Chemistry of Materials

Received: July 16, 2013
Revised: August 30, 2013
Published: September 3, 2013

   dx.doi.org/10.1021/cm402383r | *Chem. Mater.* 2014, 26, 153−162

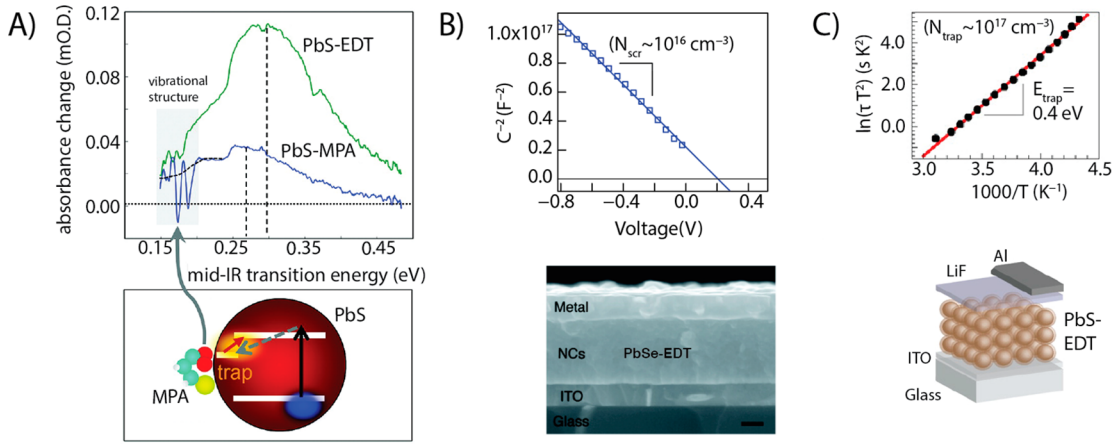

Figure 1. Characterization of nanocrystal defects in EDT treated PbS and PbSe nanocrystal thin films using (A) time-resolved infrared spectroscopy, (B) capacitance−voltage, and (C) deep level transient spectroscopy. The combination of techniques identify an average population of 10^{17} cm^{-3} acceptor traps 0.3−0.4 eV below the conduction band edge and hole populations of ~10^{16} cm^{-3}. As shown in panel A, the depth and quantity of traps can be reduced by exchanging to better passivating mercaptopropionic acid ligands. Adapted with permission from refs 17, 36, and 37. Copyright 2012, 2008, and 2013, respectively, American Chemical Society.

While control over the optical and transport properties of nanocrystal films has enabled an array of applications, including light-emitting diodes (LEDs),[21] photodetectors,[22] and photovoltaics,[23] optimization of these devices requires precise control over the doping and chemical potential of films. In this article, we highlight new insights into the electronic and chemical origin of doping within nanocrystal films, and examine an array of postsynthetic techniques, including stoichiometric control, ion impurity incorporation, and electrochemical charging, that have been concurrently developed to modulate the Fermi levels of native films. The focus of this article is on the relationship of doping treatments to the effective medium electronic properties, specifically within the context of photovoltaic applications. The history of nanocrystal doping is rich, and we refer interested readers to comprehensive reviews on doping treatments for individual nanocrystals, including incorporating magnetic defects,[24,25] plasmonic defects,[26] and optically active isovalent impurities.[27,28]

FUNDAMENTALS OF DOPING: EQUILIBRIUM AND CHARGE BALANCE

The electronic states of a semiconductor can be characterized as either being donor or acceptor in nature. Donor states are electrostatically neutral when occupied by an electron and positively charged when empty [D(+/0)], while conversely, acceptor states are neutral when empty and negatively charged when occupied [A(0/−)]. Carrier concentrations and majority carrier type emerge from the requirement to balance all of the ionized donor and acceptor states within the system,

$$p + N_D^+ = n + N_A^- \quad (1)$$

where p and N_D^+ are the concentrations of hole charge carriers and donor defects respectively, and n and N_A^- are the concentrations of conduction band electrons and acceptor defects.

At thermal equilibrium, a given donor/acceptor has an ionization probability determined by the Fermi−Dirac distribution. Themal excitation of valence electrons over the energy barrier of the bandgap results in an intrinsic carrier concentration

$$n_i = \sqrt{N_C N_V}\ \exp\left(\frac{-E_G}{2kT}\right) \quad (2)$$

where N_C and N_V are the effective density of states of the conduction band and valence band, respectively, E_G is the bandgap, k is the Boltzmann constant, and T is the temperature.[29] The intrinsic carrier concentration specifies the balance, without external excitation, between electrons and holes via the law of mass action ($np = n_i^2$). This relationship also holds for nondegenerate extrinsically doped semiconductors, as any donor/acceptor states must also be in thermal equilibrium. Defect states can shift the balance of electrons and holes, but never change the pn-product in the nondegenerate regime.

From the perspective of charge balance, it is straightforward to see how crystalline defects can give rise to ionized dopant states. For example, in a commonly studied nanocrystal such as CdSe, a cationic (Cd^{2+}) vacancy results in a net negative charge (V_{Cd}^{2-}) that is compensated by the creation of two free holes ($2p^+$). Nonstoichiometry, undercoordinated surface sites, ligands, and ionic impurities, can all shift the charge balance and cause doping within a nanocrystal film, whether it is intentional or unintentional. We will first examine sources of unintentional doping, and then move to discuss postsynthetic techniques to intentionally shift the charge balance of native films.

CHEMICAL ORIGIN OF DOPING IN NANOCRYSTAL FILMS

During a typical hot-injection synthesis, colloidal nanocrystals nucleate out of a bath of molecular precursors, monomers, and stabilizing ligands. Becase of the small crystal size, crystallographic defects suffer a higher energetic penalty and can also easily diffuse to the surface of the crystal to be removed.[30] Freshly synthesized nanocrystals typically have few bulk impurities if properly passivated, resulting in high photoluminescence (PL) yields that make them promising candidates for LEDs and biomarkers.[31,21]

Despite their relatively pure interiors, nanocrystals have extremely high surface area to volume ratios, exposing a myriad of surface defects that can produce midgap defect states.

dx.doi.org/10.1021/cm402383r | Chem. Mater. 2014, 26, 153−162

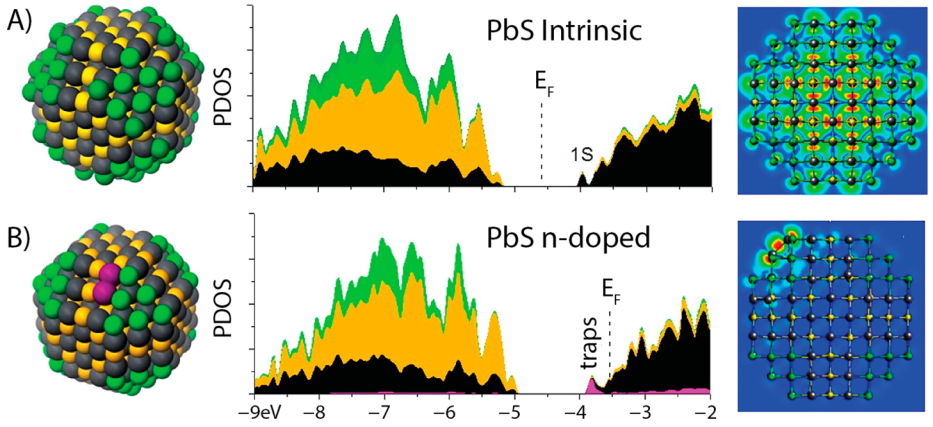

Figure 2. DFT calculations of self-compensation of a chloride capped PbS nanocrystal. Structural illustration, partial density of states (PDOS), and conduction bandedge wave functions for both a stoichiometric (A) and nonstoichiometric (B) PbS nanocrystal. Elements are color coded: Pb (black), S (sulfur), Cl (green), Pb(110) (pink). The Pb-dimer surface trap is created dynamically when the nanocrystal is n-doped through removing surface chlorides. Adapted with permission from ref 67. Copyright 2013 American Chemical Society.

Nuclear magnetic resonance (NMR) and inductively coupled plasma (ICP) spectroscopy studies show that the strong affinity between cations and nucleophilic ligands during synthesis leads to nanocrystals with nonstoichiometric cores that are charge balanced by a ligand shell.[32−35] Despite being nonstoichiometric, natively synthesized nanocrystals are not heavily doped because the excess charge of the surface cations is compensated by their binding ligands. Synthetically modifying the stoichiometry of nanocrystals is often difficult, as changing precursor concentrations can result in different sized particles instead of stoichiometric variations.

However, when native ligands are removed as part of a ligand exchange, a variety of midgap states can form and cause doping or carrier trapping depending on their depth and donor/acceptor type. A typical reaction for optoelectronic applications is the exchange of native oleate ligands with ethanedithiolate (EDT) ligands on lead chalcogenide (PbX, X = S, Se, Te) nanocrystals.[14,36] As seen in Figure 1, deep-level transient spectroscopy (DLTS) measurements show such treatments on PbSe nanocrystals produce a medium density (10^{17} cm^{-3} ≈ 1/100 NP) of acceptor states 0.4 eV below the conduction band edge.[37,38] Similar results (10^{17} cm^{-3}, 0.3 eV) are observed in PbS nanocrystals through a combination of time-resolved infrared spectroscopy (TRIR), thermal admittance spectroscopy, and transient photovoltage spectroscopy.[1,19] DLTS and photoconductive field-effect transistor (FET) measurements point to the existence of a dark low mobility state, possibly because of trap−trap hopping in a midgap band, and a high mobility state due to free carrier transport.[37,39] Indeed, EDT treated PbX nanocrystals films exhibit a p-type behavior, form Schottky junctions with low work function metals, and exhibit space charge concentrations between 10^{16}−10^{17} cm^{-3} when probed by capacitance−voltage measurements.[36,40−43]

From a stoichiometric perspective, ICP measurements show that EDT treatments shift films from being cation-rich to anion-rich.[44,45] This is in agreement with density functional theory (DFT) calculations on similar nonstoichiometric PbX nanocrystals that suggest such stoichiometry shifts lead to the generation of hole carriers to balance charge.[46,47] Excess unpassivated surface chalcogenides have also been implicated in the creation of midgap states from observations of PL quenching and recovery when switching between anion and cation capped particles.[48,49] Further, PbSe nanocrystals treated with molecular chlorine dramatically increase their PL yield because of etching of surface selenium.[50] FETs of S^{2-}-capped PbSe nanocrystals also exhibit highly p-doped behavior until passivated with atomic layer deposition infilling of alumina.[18]

In addition to exposing unpassivated surface sites, the choice of ligand also crucially determines the protection of surfaces from oxidation. Exposing EDT coated PbSe nanocrystal films to air, even briefly, creates strongly p-type and heavily conducting films due to the formation of surface oxides and superoxides.[14] In contrast, short-chain carboxylate cappings were found to be more robust.[51] Interestingly, exposure of EDT treated films to small amounts of oxygen (<0.9 Torr), lead to doping effects that are reversible upon pulling vacuum, indicating different regimes of oxidation.[52] In their attempts to tune the temporal response of PbS nanocrystal photodetectors, Konstantatos et al. elucidated the origin of these regimes by varying the capping ligand employed.[53] They found by X-ray photoelectron spectroscopy (XPS) that treating with ethanethiol removes surface lead sulfate ($PbSO_4$) that contributes to deep and long-lived surface traps, leaving only shallower and faster responding lead sulfite ($PbSO_3$) states. However, $PbSO_4$ returns after further exposure to air. Further studies demonstrate that $PbSO_4$ is responsible for oxidative doping and that its removal increases the performance of photovoltaic devices through decreasing recombination centers.[40,54] To this end, air stability of PbS nanocrystal films was finally achieved with the discovery that smaller particles (~3 nm diameter) exhibit only $PbSO_3$ as an oxidation product. Larger particles, which are more faceted and have less protected ⟨111⟩ surfaces that quickly oxidize to $PbSO_4$, leaving films too heavily doped to be useful in photovoltaic applications.[43]

Ligands can also play an active role in doping nanocrystal films, either through modulating defect depths and densities, or through acting as charge donors themselves. This field of study was galvanized by the discovery that PbSe nanocrystal films modulate from p-type to n-type when treated with the reducing agent/ligand hydrazine.[16] The effect quickly reverses as hydrazine desorbs from the film, but is also repeatable upon further exposure.[55] Despite the reducing nature of hydrazine ($E°$ = −0.41 V vs ferrocene (Fc)),[56] DFT calculations indicate that no charge transfer doping should take place with PbSe.[57] Instead, ICP measurements find hydrazine to preserve the cation-rich shell of natively synthesized particles, effectively

dx.doi.org/10.1021/cm402383r | Chem. Mater. 2014, 26, 153−162

passivating other surface sites to let the film's n-type character prevail.[44,45] Such thorough passivation played an important part in increasing the multiple exciton generation (MEG) efficiency of PbSe nanocrystal films, and eventually realizing measurable MEG photocurrent generation in a photovoltaic device.[58,59] Direct donation of charge from ligands has also been observed for silicon nanoparticles capped with cholorine.[60]

Interestingly, carrier concentrations in nanocrystal films are typically found to be much lower than expected if surface states and nonstoichiometry are the cause of doping. The effective doping concentration of a nanocrystal thin film arises from both the number of dopants per particle, and the number of particles per unit volume. Assuming a space filling fraction (ff) of 50% for randomly close packed spheres, the density of nanoparticles is,

$$n_{np} = ff * \frac{1}{V_{np}} = \mathrm{ff} * \frac{3}{4\pi {r_{np}}^3} \quad (3)$$

where V_{np} and r_{np} are the volume and radius of a spherical nanoparticle, including ligand, respectively. For a single dopant per a crystal, this would give effective doping densities in the range of $10^{20}-10^{18}$ cm^{-3} for nanocrystals with radii ranging from 1 to 5 nm. When considering the high density of surface sites per a nanocrystal, it seems unlikely that only ~1/100−1/1000 nanocrystals would contain a dopant, as would be expected from common film carrier concentrations. Perhaps a more probable scenario is one in which there exist a large concentration of defects, both dopants and traps, with a large portion of the generated carriers residing in traps. This is analogous to Fermi level pinning at semiconductor junctions, in which a large concentration of traps inhibits the movement of the Fermi level upon charge injection.[61−63]

An additional intriguing possibility exists in which nanocrystals may be self-compensating, dynamically creating traps in response to doping and charge injection. Self-doping and compensation are common in bulk films of metal oxides and chalcogenides, for example making it difficult to dope ZnO p-type.[64−66] As seen in Figure 2, DFT simulations of a PbS nanocrystal illustrate how altering the stoichiometry of the particle, while doping, also creates traps that localize the new free carriers.[67] Such phenomena are also predicted and observed in bulk semiconductors, and result in pinning of the Fermi level.[65] Experimentally, EDT treated PbS nanocrystal FETs demonstrate extremely long transient decays of conductivity after charge injection.[68] The long time scales of trapping are uncharacteristic of electronic processes, and a mechanism by which injected charges induce traps via chemical transformations has been proposed, which is similar to observations in amorphous silicon transistors.[69] Further, temperature dependent PL measurements on the same system revealed a phase transition from band emission to trap emission at a critical order−disorder transition temperature that scales with the bulk ligand melting temperature. This could support that traps are dynamically created from the movement of the surface metal−ligand complexes, or possibly be explained through temperature-activated transport to rare deep traps.[70−72] This theory is supported by DFT calculations of surface ligand diffusion that have been invoked to explain fluorescence intermittency and long-lived trap states in nanocrystals.[73]

Given the complexity of defects in nanocrystal films, it is crucial to have simple and powerful methods to intentionally modulate the Fermi level. We will now discuss recent postsynthetic approaches to this goal, including controlling the stoichiometric balance within the film, intentionally incorporating ionic impurities, and directly modulating the Fermi level with electrochemical charging.

■ STOICHIOMETRIC CONTROL

Since nonstoichiometry and charge balance are often the origin of native doping in nanocrystal films, using postsynthetic techniques to control the stoichiometry of a film is a logical tactic to control its doping. A simple, and surprisingly effective approach to this problem was discovered by Oh et al., wherein a thin layer (<4 Å) of excess cation or anion evaporated onto a nanocrystal film can shift its stoichiometry and correspondingly shifts its Fermi level.[74,44] Films of PbSe nanocrystals can be modulated between being increasingly n-type or p-type with the addition of Pb and Se, respectively, increasing from their initial concentrations of ~$10^{16}-10^{17}$ cm^{-3} holes up to ~10^{18} cm^{-3} of either carrier. The putative mechanism of this technique is that evaporated atoms bind to exposed surface sites to shift the stoichiometry of individual nanocrystals. Given the porosity of the randomly close packed film, evaporated atoms can diffuse up to ~60−80 nm, opening up possibilities for graded doping by multiple treatments.

Another approach to varying charge balance was demonstrated by the Sargent group, in which they found halide capping ligands can create stable n-type PbS nanocrystal films.[75] Contrary to what one would expect from standard reduction potentials, the level of doping increases with decreasing period (Cl > Br > I), indicating a substitutional mechanism where sulfides can more easily be substituted by similarly sized chlorides than larger iodides. Conversely, when soaked in iodide longer than bromide, larger doping and incorporation were found for iodide.[76] These effects only manifest for films treated with in air-free gloveboxes with sufficiently pure solvents such as to not form compensating oxides. Out of these observations emerges the more general insight that the overall doping effect of a given treatment can be understood by considering the average charge balance of all the atomic and molecular constituents of a film.[77] Indeed, charge accounting via Rutherford backscattering (RBS) and XPS shows a strong correlation to extracted carrier concentrations from FET measurements on films with a variety of treatments, spanning the range from 10^{18} cm^{-3} p-type to 10^{18} cm^{-3} n-type. This framework has been successfully utilized for the creation of p-n junction nanocrystal solar cells,[78] including heavily doped p-regions,[79] and n-regions with graded doping.[76]

■ ION IMPURITY DOPING

The standard industrial technique for doping semiconductors is the incorporation of ionic impurities, either through diffusion or implantation. It is thus perhaps unsurprising that this was the focus of many early doping efforts. Despite the challenges of self-purification, several successful methods have been developed to incorporate metallic and magnetic impurities, during synthesis.[80−82] As previously mentioned, many of these techniques are outside the scope of this article, which focuses on postsynthetic treatments and optoelectronic applications, and we refer readers to other comprehensive review articles.[24−27]

One approach to overcome the purification of impurities experienced at the high temperatures of synthesis is to employ

dx.doi.org/10.1021/cm402383r | Chem. Mater. 2014, 26, 153−162

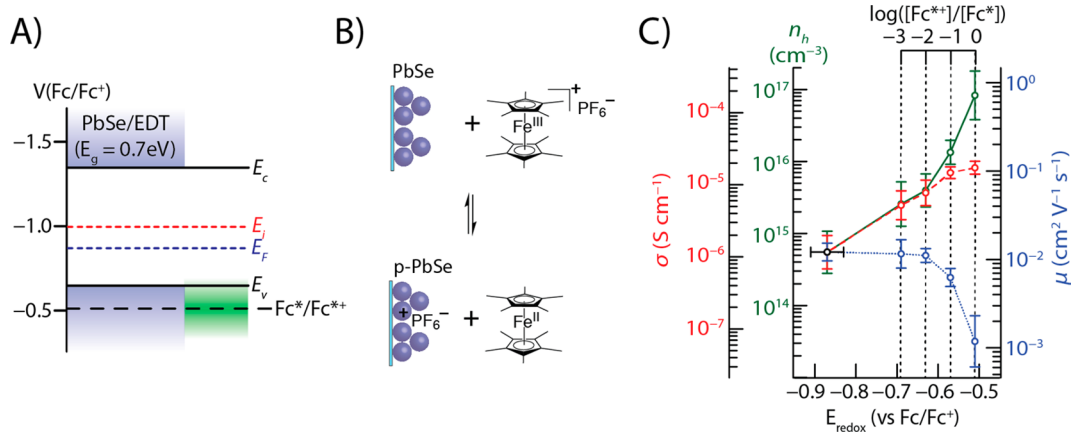

Figure 3. Doping nanocrystal films with redox buffers. (A) Energy level diagram determined from optical absorption and low-temperature cyclic voltammetry measurments. The standard reduction potential of the decamethylferrocene redox couple (Fc^*/Fc^{*+}) lies just below the PbSe nanocrystal film valence band. Regions in green mark the potentials accessible by varying the Ox/Red ratio 3 orders of magnitude in either direction. (B) Schematic of the molecular mechanism of doping. Fc^{*+} accepts an electron from the film, creating a free hole and leaving behind an intercalated PF_6^- dopant counterion to balance charge. (C) Monotonic equilibrium doping. Electrical characteristics extracted from FET measurements, conductivity (σ), mobility (μ), and hole concentration (n_h), show monotonic evolution with buffer redox potential. Carrier concentration incrementally and reversibly increases 2 orders of magnitude by varying the $[Fc^{*+}]/[Fc^*]$ ratio. Adapted with permission from ref 99. Copyright 2012, American Chemical Society.

postsynthetic cation exchange. As a low-temperature process that is driven by the free energy difference between the reactant and product phases, cation exchange is a versatile technique that allows the incorporation of a wide range of metal impurities.[83] While an age-old technique for thin films, it is also particularly effective as a size-preserving chemical transformation of nanomaterials, allowing impurities to quickly diffuse throughout the entire particle.

Typical cation exchange reactions involve immersing nanocrystals in a bath of reactants, ensuring complete transformation to the product phase. However, restricting the quantity of reactants can enact partial cation exchange, preserving the initial phase and affording a fine degree of control over the incorporated impurity density. Mocatta et al. demonstrated that exposing indium arsenide (InAs) nanocrystals to a dilute solution of Cu^+, Ag^+, or Au^{3+} ions results in the proportional incorporation of metal impurities, as measured by ICP.[84] Scanning tunneling microscopy (STM) measurements show n-type and p-type shifts of the Fermi level, corresponding to interstitial incorporation of Cu^+ and substitution with Ag^+, respectively. The interstitial location of Cu^+ impurities was later verified by X-ray absorption fine structure (XAFS) spectroscopy measurements and DFT calculations.[85] In contrast, Au^{3+} acts as an isovalent substitution for In^{3+}, perturbing the bandedge structure, but not appreciably doping the particles. While isovalent doping does not effect equilibrium carrier concentrations, the midgap states that it induces can sometimes be utilized as a charge transfer rely or optically active site, as in the case of Mn^{2+} in CdS.[27,86] Partial cation exchange has also been extended to films of nanocrystals, including CdSe[87] and PbSe,[88] with an emphasis on Ag^+ incorporation. The use of Ag^+ as a p-type dopant has even enabled optimization of PbS nanocrystal p-n junction solar cells, through creating a heavily doped p-region.[79]

Alternatively, metal impurities can be integrated into the ligands themselves, as opposed to the semiconductor lattice. By interconnecting S^{2-} capped CdSe nanocrystals with different metallic counterions, Nag et al. found that a wide variety of film properties can be modulated, including mobility, luminescence, carrier type, and catalytic properties.[89] In particular, nanocrystal films can be made increasingly p-type by reducing the charge of the connecting metal ion (In^{3+}, Cd^{2+}, K^+). This behavior is well understood in the framework of charge balance, with the metal ion acting as a substitution for a Cd^{2+} that would normally form a charge neutral matrix.

Beyond nanoscale techniques, traditional semiconductor doping strategies such as bulk diffusion are also possible. Annealing CdSe nanocrystal FETs with indium contacts causes thermal diffusion of indium atoms into the nanocrystal film, resulting in n-type doping, trap passivation, and very large (~27 $cm^2\ V^{-1}\ s^{-1}$) carrier mobilities.[90] In contrast to PbX particles, CdSe nanocrystal films are resistant to sintering up to 250 °C for 10 min, maintaining some quantum confinement in their absorption spectra, which allows for the use of temperature-assisted diffusion methods. From the vacuum deposition of the contacts, only the first 20−30 nm underneath the contacts are doped with indium, but after annealing, indium diffuses throughout the entire film.

■ ELECTROCHEMICAL METHODS

While the aforementioned techniques modulate the Fermi level of a film through the incorporation of charged defects, electrochemical approaches enable more precision through the inverse approach, whereby an imposed electrochemical potential mandates the degree of injected charge.[91] The injected free carriers, whether they are from an electrode or chemical redox agent, are accompanied by the intercalation of stable counterions (typically PF_6^- or BF_4^-) that can maintain the doping even after the applied potential is removed.

The Guyot−Sionnest group has extensively studied the effects of electrochemical charging on the optical and electrical properties of nanocrystal films.[92,93] For CdSe,[94] PbSe,[95] and HgTe,[96] they find that electrochemical cells can introduce sufficient charge to bleach the first exciton absorption due to complete $1S_e$ shell filling, create new intraband absorption peaks from free carriers, and create maxima-minima of the mobility corresponding to half and full shell filling respectively. Despite the wide range of control, the electrochemical doping

dx.doi.org/10.1021/cm402383r | Chem. Mater. 2014, 26, 153−162

becomes unstable because of parasitic reactions, possibly from traps, ligands, or dissolution of the nanocrystals themselves. As a result, all experiments must be done at low temperature to see the band edge effects. Additionally, electrochemical cells require injecting charge from an electrode, which limits their usefulness for different device architectures.

A more versatile approach would combine the precision of electrochemistry with the flexible processing of solution-based treatments. Chemical redox agents, solubilized molecular species with known reduction potentials, such as sodium biphenyl ($NaPh_2$) and cobaltocene ($CoCp_2$), have been shown to efficiently inject charge into nanocrystal films.[97,98] In the case of $CoCp_2$, PbX nanocrystal films retain high levels of injected charge for long periods of time, providing they are sufficiently passivated. However, these approaches result in high doping densities as the reactions are only stoichiometrically or kinetically restrained.

To retain the precision of electrochemical techniques, and enable equilibrium doping under thermodynamic control, both members of a redox couple must be present. In sufficient mass excess of the film, a redox couple forms a buffer, enforcing a single given electrochemical potential to the film. The potential is given by the Nernst equation

$$E_F = -q\left(E^\circ + kT \ln \frac{[Ox]}{[Red]}\right) \quad (4)$$

where E_F is the electrochemical potential of the solution, q is the elemental charge, E° is the standard reduction potential, and $[Ox]/[Red]$ is the ratio of the concentrations of oxidized and reduced forms of the redox couple. The buffer potential is modulated either by choosing a couple with a different standard reduction potential, or by varying the couple ratio. For equilibrium doping, only sufficient charge is injected into the film until the electrochemical potential difference with the buffer has been equalized.

Engel et al. have demonstrated that the application of redox buffers to nanocrystal films can produce stable, precise, and reversible doping.[99] As seen in Figure 3, when treating PbSe nanocrystal films with buffers of different ratios of decamethylferrocene/decamethyferrocenium ($[Fc^*]/[Fc^{*+}]$), the resulting doping is a monotonic function of the solution electrochemical potential, regardless of the order in which the buffers are applied. Moreover, the charging is stable upon removal from the buffer solution, as the doping occurs under equilibrium with parasitic states as well as bandedge states until the steady state value is reached. However, the degree of doping is limited by the trap states that screen the electrochemical potential difference in an analogous manner to the pinning of a Fermi level at a semiconductor metal junction.[61−63]

CHARGE BALANCE AS A PATH TO HIGHER EFFICIENCY NANOCRYSTAL PHOTOVOLTAICS

The photovoltaic effect fundamentally arises from a built-in electrochemical potential gradient, typically from an asymmetrical junction between two materials. Photogenerated carriers are separated and directed across the junction by the built-in potential gradient (V_{bi}), where they add to reservoirs of excess carriers. Under open-circuit conditions, these reservoirs shift the quasi-Fermi levels at the contacts, creating a photovoltage (V_{oc}). Since the photopotential opposes V_{bi} and reduces the ability to separate charge, V_{bi} ultimately limits V_{oc}.[100]

Silicon is an indirect bandgap semiconductor that requires thick films (300−500 μm) to maximally absorb the incident solar spectrum.[100] For photovoltaic applications, extremely low defect concentrations and long diffusion lengths are required to enable generated carriers to diffuse to the built-in junction before recombination. Nanocrystal solar cells require very different architectures, as they are typically composed of strongly absorbing materials with short carrier diffusion lengths (L_{diff}) because of their low mobilities and abundance of defects.[5,101] These thin film devices rely on the built-in electric field of the junction to assist in the extraction of photogenerated charge.

As seen in Figure 4, an illustration of a pn-junction nanocrystal solar cell with typical state of the art characteristics,

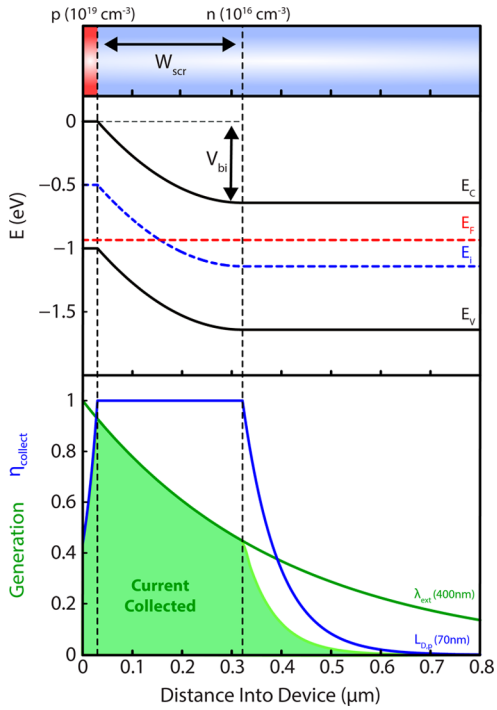

Figure 4. Schematic of an inverted structure quantum dot pn-junction solar cell with typical characteristics for state of the art PbS nanocrystal films. A p^+n junction is made between a heavily doped quantum dot p-region (10^{19} cm^{-3}) and a quantum dot n-region with moderate space charge density (10^{16} cm^{-3}).[79] The built-in potential (V_{bi}) created from the Fermi level difference between the two materials creates an electric field that bends the bands downward and is screened over the depletion width (W_{scr}). The photogenerated carrier collection probability (blue line, bottom graph), in near unity over this region since the carrier movement is assisted by drift, and drops off outside exponentially with the diffusion length (L_{diff} = 70 nm).[101] The photogeneration profile (green line, bottom graph) decays exponentially with the extinction length of 400 nm, typically for 1 μm wavelength light in a PbSe nanocrystal film.[5] The actual current collected under short-circuit (green fill, bottom graph), is the multiplication of the generation profile and collection probability, and drops significantly outside of the space charge region.

the collection efficiency drops dramatically outside of the region of built-in field, known as the space charge region. Since mobile carriers are forced out of this region by the built-in field, the field is primarily screened by the remaining immobile space charge. The width of this space charge region (W_{scr}) is thus strongly determined by the density of space charge (N_{scr})

dx.doi.org/10.1021/cm402383r | Chem. Mater. 2014, 26, 153−162

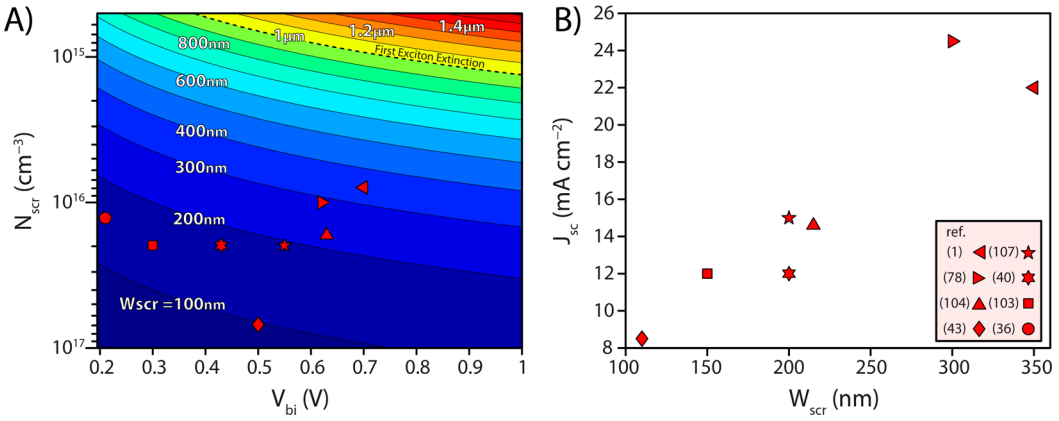

Figure 5. Literature reports (red symbols) of (A) space charge density (N_{scr}), built-in voltage (V_{bi}), in PbX nanocrystal photovoltaics. Colored contours represent space charge width (W_{scr}), are drawn from eq 5, assuming a dielectric constant of 12, and correlate well to results from literature. (B) Data from PbS films (excluding ref 36 (PbSe)), showing the strong correlation of measured space charge widths (W_{scr}) and extracted short-circuit current (J_{sc}).

$$W_{scr} = \sqrt{\frac{2\varepsilon\varepsilon_0 V_{bi}}{qN_{scr}}} \quad (5)$$

where ε is the dielectric constant, ε_0 is the permittivity of free space, and q is the fundamental charge. The "extraction length", $W_{scr} + L_{diff}$, thus forms the effective maximum thickness from which photogenerated carriers can efficiently be extracted. In the current state of the art, the majority of the extraction length is due to W_{scr} (~300 nm), however, with improved trap passivation and mobilities L_{diff} (~80 nm) can also play an important part in extracting charge.[1] Note in Figure 5b, the strong correlation between extracted current density at short-circuit (J_{sc}) and W_{scr}, which comprises most of the extraction length. Problematically, most nanocrystal solar cells have extraction lengths that are much shorter than the "extinction length", λ_{ext}, which is required to absorb most of the incoming light. In PbX nanocrystals, λ_{ext} can be ≥1 μm at wavelengths of the excitonic absorption, while the best extraction lengths currently can only reach ~300−400 nm.[1,5] Similar effects have also been observed for organic heterojunction photovoltaics.[102]

Much of the innovation that has been responsible for nanocrystal photovoltaics' rapid rise in efficiency has centered around increasing V_{bi} through varying architectures and energetics.[23] This trend is clear from examination of Figure 5a, which plots W_{scr} from literature reports as a function of V_{bi} and N_{scr}, as determined from capacitance−voltage measurements.[1,36,40,43,78,103,104,107] Since V_{bi} is determined by the initial Fermi level offset at the junction, a good deal of focus has been given to modulating the workfunction of the contacts,[36,104,105] increasing the bandgap of the absorber,[6,36,43,106] and devising new device architectures.[78,107−109] For example, heavily doping the counter electrode of a heterojunction (ZnO or TiO_2) can increase the cell voltage and reduce interfacial recombination.[110,111] Figure 5b demonstrates that these efforts have also resulted in increases of cell current, as eq 5 shows that W_{scr} is also dependent upon V_{bi}. Techniques for controlled doping of nanocrystal films have also played a role in these advances, with strongly doped regions near the contacts creating larger Fermi level shifts.[76,79,112]

Examination of Figure 5 reveals that large gains in W_{scr} and thus J_{sc} are possible via reductions in N_{scr}. This is equivalent to making the film more intrinsic, as in a PIN or graded doping type architecture. Such designs are essential to maintain V_{bi} and thus V_{oc} as the Fermi level in the absorber layer is moved toward the midgap. This brings the additional engineering challenge of designing methods that can be employed a layer-by-layer fashion, or alternatively solution based doping techniques robust enough to be maintained after ligand exchange. One approach to this end is to devise better methods of passivation, and indeed, some of the best performing devices to date rely on novel passivation strategies.[1,17,113]

Unexplored territory exists, however, in the possibility of compensating native space charge with comparable amounts of immobile charge of opposite polarity. Even a modest result, reducing the charge density by a factor of 10 has, the potential to create cells with W_{scr} greater than the 1 μm needed to absorb most of the incident solar spectrum. In particular, we note that while precisely doping a film to compensate its native charge may be difficult for kinetically or stoichiometrically limited methods, electrochemical techniques such as redox buffers may be uniquely suited to the challenge, as the appropriate amount of charge is automatically injected as required to produce a desired change in the Fermi level.

SUMMARY AND OUTLOOK

In summary, a large variety of techniques are now accessible to perturb and control carrier concentrations in nanocrystal films. The preservation of nanocrystal size and film morphology during these treatments ensures that the optical and transport properties are largely maintained. Doping of the effective medium originates from nonstoichiometry, ligands and unpassivated surface sites, which shift the balance of space charge within the film and generate free carriers. Simultaneously, many of the free carriers are likely localized to traps of similar chemical origin, possibly due to self-compensation, and the Fermi level is often pinned. Despite this, a broad range of electrochemical potential shifts can be induced in native films through methods based on stoichiometric control, metal ion incorporation, and electrochemical charging. These advances have led to improvements in nanocrystal photovoltaic performance, enabling architectures such as pn-junction, heavily doped heterojunctions, and graded junctions. These advances have led to increased cell voltages and incremental improvements in the width of the space charge region. We have highlighted the potential for charge balance in the absorber layer, whether

dx.doi.org/10.1021/cm402383r | Chem. Mater. 2014, 26, 153−162

through native passivation or postsynthetic compensation, to extend the extraction length. Further improvements in doping and processing have the potential to realize such PIN architectures and enable thicker and more efficient nanocrystal photovoltaics.

AUTHOR INFORMATION

Corresponding Author

*E-mail: alivis@berkeley.edu.

Author Contributions

The manuscript was written through contributions of all authors. All authors have given approval to the final version of the manuscript.

Notes

The authors declare no competing financial interest.

Biographies

Jesse Engel received a B.A. in Physics from the University of California Berkeley in 2006. In 2013, he received his Ph.D in Materials Science and Engineering from the University of California Berkeley in the laboratory of Paul Alivisatos, where he studied the controlled doping of semiconductor nanocrystals. He is currently a joint postdoc at Stanford and U.C. Berkeley, studying neuromorphic engineering with professors H.-S. Phillip Wong and Bruno Olshausen.

Paul Alivisatos is currently the Larry and Diane Bock Professor of Nanotechnology at the University of California Berkeley and serves as the seventh director of Lawrence Berkeley National Laboratory. He received a Bachelor's degree in Chemistry from the University of Chicago in 1981 and a Ph.D. in Chemistry from U.C. Berkeley in 1986 prior to postdoctoral work with Louis Brus at AT&T Bell Labs. He is a member of the National Academy of Sciences, the American Academy of Arts and Science, a fellow of the AAAS, ACS, APS, and MRS, and the Co-Editor of Nano Letters.

ACKNOWLEDGMENTS

The authors gratefully acknowledge financial support by DOE NSET program on the Self-Assembly of Organic/Inorganic Nanocomposite Materials (Grant DE-AC02-05CH11231 to A.P.A), under which all work for this publication was supported.

REFERENCES

(1) Ip, A. H.; Thon, S. M.; Hoogland, S.; Voznyy, O.; Zhitomirsky, D.; Debnath, R.; Levina, L.; Rollny, L. R.; Carey, G. H.; Fischer, A.; Kemp, K. W.; Kramer, I. J.; Ning, Z.; Labelle, A. J.; Chou, K. W.; Amassian, A.; Sargent, E. H. *Nat. Nanotechnol.* **2012**, *7*, 577−582.

(2) Kramer, I. J.; Sargent, E. H. *ACS Nano* **2011**, *5*, 8506−8514.

(3) Talapin, D. V; Lee, J.-S.; Kovalenko, M. V; Shevchenko, E. V *Chem. Rev.* **2010**, *110*, 389−458.

(4) Wang, Z.; Schliehe, C.; Bian, K.; Dale, D.; Bassett, W. A.; Hanrath, T.; Klinke, C.; Weller, H. *Nano Lett.* **2013**, *13*, 1303−1311.

(5) Law, M.; Beard, M. C.; Choi, S.; Luther, J. M.; Hanna, M. C.; Nozik, A. J. *Nano Lett.* **2008**, *8*, 3904−3910.

(6) Ma, W.; Swisher, S. L.; Ewers, T.; Engel, J.; Ferry, V. E.; Atwater, H. A.; Alivisatos, A. P. *ACS Nano* **2011**, *5*, 8140−8147.

(7) Moreels, I.; Lambert, K.; Smeets, D.; De Muynck, D.; Nollet, T.; Martins, J. C.; Vanhaecke, F.; Vantomme, A.; Delerue, C.; Allan, G.; Hens, Z. *ACS Nano* **2009**, *3*, 3023−3030.

(8) Geiregat, P.; Justo, Y.; Abe, S.; Flamee, S.; Hens, Z. *ACS Nano* **2013**, *7*, 987−993.

(9) Alivisatos, A. P. *J. Phys. Chem.* **1996**, *100*, 13226−13239.

(10) Moreels, I.; Allan, G.; De Geyter, B.; Wirtz, L.; Delerue, C.; Hens, Z. *Phys. Rev. B* **2010**, *81*, No. 235319.

(11) Wolcott, A.; Doyeux, V.; Nelson, C. A.; Gearba, R.; Lei, K. W.; Yager, K. G.; Dolocan, A. D.; Williams, K.; Nguyen, D.; Zhu, X.-Y. *J. Phys. Chem. Lett.* **2011**, *2*, 795−800.

(12) Steckel, J. S.; Yen, B. K. H.; Oertel, D. C.; Bawendi, M. G. *J. Am. Chem. Soc.* **2006**, *128*, 13032−13033.

(13) Peng, X.; Manna, L.; Yang, W.; Wickham, J.; Scher, E.; Kadavanich, A.; Alivisatos, A. *Nature* **2000**, *404*, 59−61.

(14) Luther, J. M.; Law, M.; Song, Q.; Perkins, C. L.; Beard, M. C.; Nozik, A. J. *ACS Nano* **2008**, *2*, 271−280.

(15) Koh, W.-K.; Saudari, S. R.; Fafarman, A. T.; Kagan, C. R.; Murray, C. B. *Nano Lett.* **2011**, *11*, 4764−4767.

(16) Talapin, D. V; Murray, C. B. *Science* **2005**, *310*, 86−9.

(17) Jeong, K. S.; Tang, J.; Liu, H.; Kim, J.; Schaefer, A. W.; Kemp, K.; Levina, L.; Wang, X.; Hoogland, S.; Debnath, R.; Brzozowski, L.; Sargent, E. H.; Asbury, J. B. *ACS Nano* **2012**, *6*, 89−99.

(18) Liu, Y.; Tolentino, J.; Gibbs, M.; Ihly, R.; Perkins, C. L.; Liu, Y.; Crawford, N.; Hemminger, J. C.; Law, M. *Nano Lett.* **2013**, *13*, 1578−1587.

(19) Tang, J.; Kemp, K. W.; Hoogland, S.; Jeong, K. S.; Liu, H.; Levina, L.; Furukawa, M.; Wang, X.; Debnath, R.; Cha, D.; Chou, K. W.; Fischer, A.; Amassian, A.; Asbury, J. B.; Sargent, E. H. *Nat. Mater.* **2011**, *10*, 765−771.

(20) Stauffer, D.; Aharony, A. *Introduction to Percolation Theory*; 2nd ed.; Taylor & Francis: London, 2003.

(21) Shirasaki, Y.; Supran, G. J.; Bawendi, M. G.; Bulović, V. *Nat. Photonics* **2012**, *7*, 13−23.

(22) McDonald, S. A.; Konstantatos, G.; Zhang, S.; Cyr, P. W.; Klem, E. J. D.; Levina, L.; Sargent, E. H. *Nat. Mater.* **2005**, *4*, 138−142.

(23) Tang, J.; Sargent, E. H. *Adv. Mater.* **2011**, *23*, 12−29.

(24) Norris, D. J.; Efros, A. L.; Erwin, S. C. *Science* **2008**, *319*, 1776−9.

(25) Beaulac, R.; Ochsenbein, S. T.; Gamelin, D. R. In *Nanocrystal Quantum Dots*; Klimov, V. I., Ed.; Taylor & Francis: New York, NY, 2010.

(26) Buonsanti, R.; Milliron, D. J. *Chem. Mater.* **2013**, *25*, 1305−1317.

(27) Pradhan, N.; Sarma, D. D. *J. Phys. Chem. Lett.* **2011**, *2*, 2818−2826.

(28) Jana, S.; Srivastava, B. B.; Jana, S.; Bose, R.; Pradhan, N. *J. Phys. Chem. Lett.* **2012**, *3*, 2535−2540.

(29) Sze, S. M.; Ng, K. K. *Physics of Semiconductor Devices*, 3rd ed.; John Wiley & Sons Inc.: Hoboken, NJ, 2007.

(30) Dalpian, G.; Chelikowsky, J. *Phys. Rev. Lett.* **2006**, *96*, No. 226802.

(31) Bruchez, M., Jr.; Morrone, M.; Gin, P.; Weiss, S.; Alivisatos, P. *Science* **1998**, *281*, 2013−2016.

(32) Moreels, I.; Fritzinger, B.; Martins, J. C.; Hens, Z. *J. Am. Chem. Soc.* **2008**, *130*, 15081−15086.

(33) Moreels, I.; Lambert, K.; De Muynck, D.; Vanhaecke, F.; Poelman, D.; Martins, J. C.; Allan, G.; Hens, Z. *Chem. Mater.* **2007**, *19*, 6101−6106.

(34) Morris-Cohen, A. J.; Frederick, M. T.; Lilly, G. D.; McArthur, E. A.; Weiss, E. A. *J. Phys. Chem. Lett.* **2010**, *1*, 1078−1081.

(35) Smith, D. K.; Luther, J. M.; Semonin, O. E.; Nozik, A. J.; Beard, M. C. *ACS Nano* **2011**, *5*, 183−190.

(36) Luther, J. M.; Law, M.; Beard, M. C.; Song, Q.; Reese, M. O.; Ellingson, R. J.; Nozik, A. J. *Nano Lett.* **2008**, *8*, 3488−3492.

(37) Bozyigit, D.; Jakob, M.; Yarema, O.; Wood, V. *ACS Appl. Mater. Interfaces* **2013**, *5*, 2915−2919.

(38) Lang, D. V. *J. Appl. Phys.* **1974**, *45*, 3023.

(39) Nagpal, P.; Klimov, V. I. *Nat. Commun.* **2011**, *2*, 486.

(40) Barkhouse, A. R.; Pattantyus-Abraham, A. G.; Levina, L.; Sargent, E. H. *ACS Nano* **2008**, *2*, 2356−2362.

(41) Johnston, K. W.; Pattantyus-Abraham, A. G.; Clifford, J. P.; Myrskog, S. H.; MacNeil, D. D.; Levina, L.; Sargent, E. H. *Appl. Phys. Lett.* **2008**, *92*, No. 151115.

(42) Johnston, K. W.; Pattantyus-Abraham, A. G.; Clifford, J. P.; Myrskog, S. H.; Hoogland, S.; Shukla, H.; Klem, E. J. D.; Levina, L.; Sargent, E. H. *Appl. Phys. Lett.* **2008**, *92*, No. 122111.

(43) Tang, J.; Brzozowski, L.; Barkhouse, A. R.; Wang, X.; Debnath, R.; Wolowiec, R.; Palmiano, E.; Levina, L.; Pattantyus-Abraham, A. G.; Jamakosmanovic, D.; Sargent, E. H. *ACS Nano* **2010**, *4*, 869−878.
(44) Luther, J. M.; Pietryga, J. M. *ACS Nano* **2013**, *7*, 1845−1849.
(45) Hughes, B. K.; Ruddy, D. A.; Blackburn, J. L.; Smith, D. K.; Bergren, M. R.; Nozik, A. J.; Johnson, J. C.; Beard, M. C. *ACS Nano* **2012**, *6*, 5498−1506.
(46) Kim, D.; Kim, D.-H.; Lee, J.-H.; Grossman, J. C. *Phys. Rev. Lett.* **2013**, *110*, No. 196802.
(47) Gai, Y.; Peng, H.; Li, J. *J. Phys. Chem. C* **2009**, *113*, 21506−21511.
(48) Wei, H. H.-Y.; Evans, C. M.; Swartz, B. D.; Neukirch, A. J.; Young, J.; Prezhdo, O. V; Krauss, T. D. *Nano Lett.* **2012**, *12*, 4465−4471.
(49) Jasieniak, J.; Mulvaney, P. *J. Am. Chem. Soc.* **2007**, *129*, 2841−2848.
(50) Bae, W. K.; Joo, J.; Padilha, L. A.; Won, J.; Lee, D. C.; Lin, Q.; Koh, W.; Luo, H.; Klimov, V. I.; Pietryga, J. M. *J. Am. Chem. Soc.* **2012**, *134*, 20160−20168.
(51) Zarghami, M. H.; Liu, Y.; Gibbs, M.; Gebremichael, E.; Webster, C.; Law, M. *ACS Nano* **2010**, *4*, 2475−2485.
(52) Leschkies, K. S.; Kang, M. S.; Aydil, E. S.; Norris, D. J. *J. Phys. Chem. C* **2010**, *114*, 9988−9996.
(53) Konstantatos, G.; Levina, L.; Fischer, A.; Sargent, E. H. *Nano Lett.* **2008**, *8*, 1446−1450.
(54) Klem, E. J. D.; Shukla, H.; Hinds, S.; MacNeil, D. D.; Levina, L.; Sargent, E. H. *Appl. Phys. Lett.* **2008**, *92*, No. 212105.
(55) Wang, R. Y.; Feser, J. P.; Lee, J.-S.; Talapin, D. V; Segalman, R.; Majumdar, A. *Nano Lett.* **2008**, *8*, 2283−2288.
(56) Connelly, N. G.; Geiger, W. E. *Chem. Rev.* **1996**, *96*, 877−910.
(57) Kutana, A.; Erwin, S. C. *Phys. Rev. B* **2011**, *83*, No. 235419.
(58) Beard, M. C.; Midgett, A. G.; Law, M.; Semonin, O. E.; Ellingson, R. J.; Nozik, A. J. *Nano Lett.* **2009**, *9*, 836−845.
(59) Semonin, O. E.; Luther, J. M.; Choi, S.; Chen, H.-Y.; Gao, J.; Nozik, A. J.; Beard, M. C. *Science* **2011**, *334*, 1530−1533.
(60) Wheeler, L. M.; Neale, N. R.; Chen, T.; Kortshagen, U. R. *Nat. Commun.* **2013**, *4*, 2197.
(61) Van Meirhaeghe, R. L.; Cardon, F.; Gomes, W. P. *J. Electroanal. Chem. Interfacial Electrochem.* **1985**, *188*, 287−291.
(62) Lewerenz, H. J. *J. Electroanal. Chem.* **1993**, *356*, 121−143.
(63) Bard, A. J.; Bocarsly, A. B.; Fan, F. R. F.; Walton, E. G.; Wrighton, M. S. *J. Am. Chem. Soc.* **1980**, *102*, 3671−3677.
(64) Park, C. H.; Zhang, S. B.; Wei, S.-H. *Phys. Rev. B* **2002**, *66*, No. 073202.
(65) Zunger, A. *Appl. Phys. Lett.* **2003**, *83*, 57.
(66) Zhang, X.; Zhang, L. *J. Phys. Chem. C* **2010**, *114*, 18198−18206.
(67) Voznyy, O.; Thon, S. M.; Ip, A. H.; Sargent, E. H. *J. Phys. Chem. Lett.* **2013**, 987−992.
(68) Osedach, T. P.; Zhao, N.; Andrew, T. L.; Brown, P. R.; Wanger, D. D.; Strasfeld, D. B.; Chang, L.-Y.; Bawendi, M. G.; Bulović, V. *ACS Nano* **2012**, *6*, 3121−3127.
(69) Deane, S.; Wehrspohn, R.; Powell, M. *Phys. Rev. B* **1998**, *58*, 12625−12628.
(70) Nelson, C. A.; Zhu, X.-Y. *J. Am. Chem. Soc.* **2012**, *134*, 7592−7595.
(71) Moroz, P.; Kholmicheva, N.; Mellott, B.; Liyanage, G.; Rijal, U.; Bastola, E.; Huband, K.; Khon, E.; McBride, K.; Zamkov, M. *ACS Nano* **2013**, *7*, 6964−6977.
(72) Zhitomirsky, D.; Kramer, I. J.; Labelle, A. J.; Fischer, A.; Debnath, R.; Pan, J.; Bakr, O. M.; Sargent, E. H. *Nano Lett.* **2012**, *12*, 1007−1012.
(73) Voznyy, O. *J. Phys. Chem. C* **2011**, *115*, 15927−15932.
(74) Oh, S. J.; Berry, N. E.; Choi, J.-H.; Gaulding, E. A.; Paik, T.; Hong, S.-H.; Murray, C. B.; Kagan, C. R. *ACS Nano* **2013**, *7*, 2413−2421.
(75) Zhitomirsky, D.; Furukawa, M.; Tang, J.; Stadler, P.; Hoogland, S.; Voznyy, O.; Liu, H.; Sargent, E. H. *Adv. Mater.* **2012**, *24*, 6181−6185.
(76) Ning, Z.; Zhitomirsky, D.; Adinolfi, V.; Sutherland, B.; Xu, J.; Voznyy, O.; Maraghechi, P.; Lan, X.; Hoogland, S.; Ren, Y.; Sargent, E. H. *Adv. Mater.* **2013**, *25*, 1719−1723.
(77) Voznyy, O.; Zhitomirsky, D.; Stadler, P.; Ning, Z.; Hoogland, S.; Sargent, E. H. *ACS Nano* **2012**, *6*, 8448−8455.
(78) Tang, J.; Liu, H.; Zhitomirsky, D.; Hoogland, S.; Wang, X.; Furukawa, M.; Levina, L.; Sargent, E. H. *Nano Lett.* **2012**, *12*, 4889−4894.
(79) Liu, H.; Zhitomirsky, D.; Hoogland, S.; Tang, J.; Kramer, I. J.; Ning, Z.; Sargent, E. H. *Appl. Phys. Lett.* **2012**, *101*, No. 151112.
(80) Erwin, S. C.; Zu, L.; Haftel, M. I.; Efros, A. L.; Kennedy, T. A.; Norris, D. J. *Nature* **2005**, *436*, 91−94.
(81) Buonsanti, R.; Llordes, A.; Aloni, S.; Helms, B. A.; Milliron, D. J. *Nano Lett.* **2011**, *11*, 4706−4710.
(82) Norberg, N. S.; Kittilstved, K. R.; Amonette, J. E.; Kukkadapu, R. K.; Schwartz, D. A.; Gamelin, D. R. *J. Am. Chem. Soc.* **2004**, *126*, 9387−9398.
(83) Rivest, J. B.; Jain, P. K. *Chem. Soc. Rev.* **2013**, *42*, 89−96.
(84) Mocatta, D.; Cohen, G.; Schattner, J.; Millo, O.; Rabani, E.; Banin, U. *Science* **2011**, *332*, 77−81.
(85) Amit, Y.; Eshet, H.; Faust, A.; Patllola, A.; Rabani, E.; Banin, U.; Frenkel, A. I. *J. Phys. Chem. C* **2013**, 13688−13696.
(86) Santra, P. K.; Kamat, P. V *J. Am. Chem. Soc.* **2012**, *134*, 2508−2511.
(87) Sahu, A.; Kang, M. S.; Kompch, A.; Notthoff, C.; Wills, A. W.; Deng, D.; Winterer, M.; Frisbie, C. D.; Norris, D. J. *Nano Lett.* **2012**, *12*, 2587−2594.
(88) Kang, M. S.; Sahu, A.; Frisbie, C. D.; Norris, D. J. *Adv. Mater.* **2013**, *25*, 725−731.
(89) Nag, A.; Chung, D. S.; Dolzhnikov, D. S.; Dimitrijevic, N. M.; Chattopadhyay, S.; Shibata, T.; Talapin, D. V *J. Am. Chem. Soc.* **2012**, *134*, 13604−13615.
(90) Choi, J.-H.; Fafarman, A. T.; Oh, S. J.; Ko, D.-K.; Kim, D. K.; Diroll, B. T.; Muramoto, S.; Gillen, J. G.; Murray, C. B.; Kagan, C. R. *Nano Lett.* **2012**, *12*, 2631−2638.
(91) Rajeshwar, K. *Fundamentals of Semiconductor Electrochemistry and Photoelectrochemistry*; Bard, A. J., Licht, S., Stratmann, M., Eds.; Wiley-VCH: Weinheim, Germany, 2001.
(92) Guyot-Sionnest, P. *Microchim. Acta* **2008**, *160*, 309−314.
(93) Yu, D.; Wang, C.; Wehrenberg, B.; Guyot-Sionnest, P. *Phys. Rev. Lett.* **2004**, *92*, No. 216802.
(94) Yu, D.; Wang, C.; Guyot-Sionnest, P. *Science* **2003**, *300*, 1277−1280.
(95) Wehrenberg, B. L.; Yu, D.; Ma, J.; Guyot-Sionnest, P. *J. Phys. Chem. B* **2005**, *109*, 20192−20199.
(96) Liu, H.; Keuleyan, S.; Guyot-Sionnest, P. *J. Phys. Chem. C* **2012**, *116*, 1344−1349.
(97) Shim, M.; Guyot-Sionnest, P. *Nature* **2000**, *407*, 981−3.
(98) Koh, W.-K.; Koposov, A. Y.; Stewart, J. T.; Pal, B. N.; Robel, I.; Pietryga, J. M.; Klimov, V. I. *Sci. Rep.* **2013**, *3*, 2004.
(99) Engel, J. H.; Surendranath, Y.; Alivisatos, A. P. *J. Am. Chem. Soc.* **2012**, *134*, 13200−13203.
(100) Nelson, J. *The Physics of Solar Cells*; Imperial College Press: London, 2003.
(101) Zhitomirsky, D.; Voznyy, O.; Hoogland, S.; Sargent, E. H. *ACS Nano* **2013**, *7*, 5282−5290.
(102) Kirchartz, T.; Agostinelli, T.; Campoy-Quiles, M.; Gong, W.; Nelson, J. *J. Phys. Chem. Lett.* **2012**, *3*, 3470−3475.
(103) Clifford, J. P.; Johnston, K. W.; Levina, L.; Sargent, E. H. *Appl. Phys. Lett.* **2007**, *91*, No. 253117.
(104) Brown, P. R.; Lunt, R. R.; Zhao, N.; Osedach, T. P.; Wanger, D. D.; Chang, L.-Y.; Bawendi, M. G.; Bulović, V. *Nano Lett.* **2011**, *11*, 2955−2961.
(105) Gao, J.; Perkins, C. L.; Luther, J. M.; Hanna, M. C.; Chen, H.-Y.; Semonin, O. E.; Nozik, A. J.; Ellingson, R. J.; Beard, M. C. *Nano Lett.* **2011**, *11*, 3263−3266.
(106) Gao, J.; Luther, J. M.; Semonin, O. E.; Ellingson, R. J.; Nozik, A. J.; Beard, M. C. *Nano Lett.* **2011**, *11*, 1002−1008.

(107) Pattantyus-Abraham, A. G.; Kramer, I. J.; Barkhouse, A. R.; Wang, X.; Konstantatos, G.; Debnath, R.; Levina, L.; Raabe, I.; Nazeeruddin, M. K.; Grätzel, M.; Sargent, E. H. *ACS Nano* **2010**, *4*, 3374−3380.
(108) Luther, J. M.; Gao, J.; Lloyd, M. T.; Semonin, O. E.; Beard, M. C.; Nozik, A. J. *Adv. Mater.* **2010**, *22*, 3704−3707.
(109) Choi, J. J.; Lim, Y.-F.; Santiago-Berrios, M. B.; Oh, M.; Hyun, B.-R.; Sun, L.; Bartnik, A. C.; Goedhart, A.; Malliaras, G. G.; Abruña, H. D.; Wise, F. W.; Hanrath, T. *Nano Lett.* **2009**, *9*, 3749−3755.
(110) Koleilat, G. I.; Wang, X.; Labelle, A. J.; Ip, A. H.; Carey, G. H.; Fischer, A.; Levina, L.; Brzozowski, L.; Sargent, E. H. *Nano Lett.* **2011**, *11*, 5173−5178.
(111) Ehrler, B.; Musselman, K. P.; Böhm, M. L.; Morgenstern, F. S. F.; Vaynzof, Y.; Walker, B. J.; Macmanus-Driscoll, J. L.; Greenham, N. C. *ACS Nano* **2013**, *7*, 4210−4220.
(112) Maraghechi, P.; Labelle, A. J.; Kirmani, A. R.; Lan, X.; Adachi, M. M.; Thon, S. M.; Hoogland, S.; Lee, A.; Ning, Z.; Fischer, A.; Amassian, A.; Sargent, E. H. *ACS Nano* **2013**, *7*, 6111−6116.
(113) Liu, Y.; Gibbs, M.; Perkins, C. L.; Tolentino, J.; Zarghami, M. H.; Bustamante, J.; Law, M. *Nano Lett.* **2011**, *11*, 5349−55.